Time-resolved luminescence resonance energy transfer imaging of protein–protein interactions in living cells

Harsha E. Rajapakse[a], Nivriti Gahlaut[a], Shabnam Mohandessi[a], Dan Yu[b], Jerrold R. Turner[b], and Lawrence W. Miller[a,1]

[a]Department of Chemistry, University of Illinois, Chicago, IL 60607; and [b]Department of Pathology, University of Chicago, Chicago, IL 60637

Edited by Barbara Imperiali, Massachusetts Institute of Technology, Cambridge, MA, and approved June 28, 2010 (received for review February 18, 2010)

Förster resonance energy transfer (FRET) with fluorescent proteins permits high spatial resolution imaging of protein–protein interactions in living cells. However, substantial non-FRET fluorescence background can obscure small FRET signals, making many potential interactions unobservable by conventional FRET techniques. Here we demonstrate time-resolved microscopy of luminescence resonance energy transfer (LRET) for live-cell imaging of protein–protein interactions. A luminescent terbium complex, TMP-Lumi4, was introduced into cultured cells using two methods: (*i*) osmotic lysis of pinocytic vesicles; and (*ii*) reversible membrane permeabilization with streptolysin O. Upon intracellular delivery, the complex was observed to bind specifically and stably to transgenically expressed *Escherichia coli* dihydrofolate reductase (eDHFR) fusion proteins. LRET between the eDHFR-bound terbium complex and green fluorescent protein (GFP) was detected as long-lifetime, sensitized GFP emission. Background signals from cellular autofluorescence and directly excited GFP fluorescence were effectively eliminated by imposing a time delay (10 μs) between excitation and detection. Background elimination made it possible to detect interactions between the first PDZ domain of ZO-1 (fused to eDHFR) and the C-terminal YV motif of claudin-1 (fused to GFP) in single microscope images at subsecond time scales. We observed a highly significant ($P < 10^{-6}$), six-fold difference between the mean, donor-normalized LRET signal from cells expressing interacting fusion proteins and from control cells expressing noninteracting mutants. The results show that time-resolved LRET microscopy with a selectively targeted, luminescent terbium protein label affords improved speed and sensitivity over conventional FRET methods for a variety of live-cell imaging and screening applications.

cellular imaging | dihydrofolate reductase | Forster resonance energy transfer | lanthanide luminescence | protein labeling

Protein–protein interactions, often mediated by modular interaction domains, play a fundamental role in the dynamic organization of cells (1). Various experimental techniques such as immunoprecipitation, affinity chromatography, and yeast two-hybrid analysis have been used to identify putatively interacting proteins and deduce the biomolecular mechanisms of cell function (2, 3). However, cell-free studies and screening assays do not provide information about the spatio-temporal organization of protein networks in the natural environment of the living cell or organism. A variety of optical methods are available for monitoring protein interactions in cells, including fluorescence cross correlation spectroscopy (FCCS) (4, 5), bimolecular fluorescence complementation (6), translocation-based assays (7–9), and methods that detect intermolecular Förster resonance energy transfer (FRET). Among these methods, only FRET allows dynamic and reversible imaging of protein–protein interactions while simultaneously preserving information about their subcellular distribution (10–12).

FRET occurs when a fluorescent donor molecule is brought within close proximity (<10 nm) to an acceptor whose absorption spectrum overlaps with the donor emission spectrum. FRET can be detected in appropriately configured microscopes as a decrease in the fluorescence intensity, lifetime, or anisotropy of the donor or as an increase in the fluorescence intensity of the acceptor upon donor excitation (if the acceptor is fluorescent). Fluorescent proteins (FPs), especially cyan (CFP) and yellow (YFP) variants, are the most common donors and acceptors used in live-cell FRET imaging (13). Intermolecular FRET between two FP-labeled proteins has been used to visualize receptor oligomerization and interactions between transcription factors and cell signaling components (11, 13–15).

Steady-state monitoring of sensitized acceptor emission upon donor excitation is the most popular FRET microscopy method. This technique involves acquiring three sets of images using different filter combinations: donor excitation/donor emission, acceptor excitation/acceptor emission, and donor excitation/acceptor emission (11, 12, 16, 17). The images are then processed postacquisition to correct for cross-detection of donor fluorescence in the acceptor emission channel (and vice versa), and to normalize for the dependence of FRET on the relative concentrations of donor and acceptor. However, image processing propagates noise and uncertainty from each individual image, lowering the sensitivity and precision of steady-state FRET imaging. Changes in donor emission intensity upon acceptor photobleaching enable direct determination of FRET efficiency (the fraction of the photon energy absorbed by the donor that is transferred to the acceptor), but this method destroys the sample and precludes time-lapse imaging. Alternatively, fluorescence lifetime imaging microscopy (FLIM) allows direct detection of FRET effects on donor excited-state lifetime and, therefore, overcomes artifacts associated with donor/acceptor spectral overlap. However, FLIM image acquisition can take several minutes and requires complicated, expensive instrumentation to accurately resolve changes in nanosecond-scale lifetimes of FPs or organic fluorophores (11). Finally, the maximum FRET dynamic range for nondimerizing fluorescent proteins is <5-fold (11, 18), and the signal observed by microscopy in living cells may only change ~10% (14, 15). The small signal variation and considerable noise factors make many interactions difficult or impossible to measure by existing FRET approaches. Therefore, despite numerous reported successes, FRET imaging has significant limitations.

Lanthanide coordination complexes are well established probes for detecting biomolecular interactions in cell-free systems at high signal-to-background ratio (19–22). As lanthanide emission is not technically fluorescence (singlet-to-singlet transi-

Author contributions: J.R.T. and L.W.M. designed research; H.E.R. performed research; N.G., S.M., and D.Y. contributed new reagents/analytic tools; H.E.R. and L.W.M. analyzed data; and H.E.R., J.R.T., and L.W.M. wrote the paper.

Conflict of interest statement: L.W.M. is a coinventor on a patent relevant to this work (US Patent 7575866) and inventor on a relevant provisional patent application filed by the University of Illinois at Chicago.

This article is a PNAS Direct Submission.

[1]To whom correspondence should be addressed. E-mail: lwm2006@uic.edu.

This article contains supporting information online at www.pnas.org/lookup/suppl/doi:10.1073/pnas.1002025107/-/DCSupplemental.

tion), the term luminescence (or lanthanide-based) resonance energy transfer (LRET) is commonly used to describe transfer from a lanthanide donor to an organic fluorophore or fluorescent protein acceptor. Lanthanide complexes have two distinct properties that enable sensitive LRET measurements. Firstly, large Stokes shifts (separation between excitation and emission wavelengths) and narrow emission lines facilitate efficient spectral separation of donor and acceptor emission signals. Secondly, long-lived (μs-ms) luminescence enables time-resolved detection, where pulsed light excites the sample, and the detector is switched on after decay of short-lived (<100 ns) autofluorescence and directly excited acceptor fluorescence background signals (21). Direct conjugation of terbium or europium complexes to oligonucleotides, antibodies and proteins has permitted the development of sensitive time-resolved LRET assays of biomolecular interactions in purified biochemical preparations, cellular extracts, and on cell surfaces (22–24). Recently, lanthanide complexes have been developed as probes for live cell imaging applications using time-resolved microscopy with pulsed, near-UV single photon or two photon excitation (25–28). Time-resolved microscopy in the microsecond domain has also been demonstrated using platinum or palladium complexes (29–31). However, to date, lanthanide complexes have not been used as LRET donors for intracellular experiments because: (*i*) suitably bright and photostable complexes were not available; (*ii*) methods to deliver membrane-impermeant lanthanide complexes from culture medium to the cytoplasm were lacking; and (*iii*) novel approaches were needed to specifically attach probes to proteins or subcellular structures.

Herein we report LRET imaging of protein–protein interactions in living cells. We show that a luminescent terbium complex, TMP-Lumi4, can be delivered to the cytoplasm and specifically targeted to *Escherichia coli* dihydrofolate reductase (eDHFR) fusion proteins. Time-resolved microscopy was used to image LRET between the terbium complex and green fluorescent protein (GFP) by detecting long-lifetime (>10 μs) terbium-sensitized GFP emission (Fig. 1). Interactions between the first PDZ domain of ZO-1 and the C-terminal YV motif of claudin-1 were detected unambiguously in a single microscope image at time scales (seconds) comparable to steady-state FRET imaging, but without the need for multiple control measurements and associated postimage processing. Whereas steady-state microscopy of intermolecular FRET may yield signal changes of only 10% (14, 15), we observed >6-fold change in mean, donor-normalized LRET signal between cells expressing interacting proteins and control cells expressing noninteracting mutants. This article shows that time-resolved LRET microscopy enables faster, more sensitive and simpler analyses of molecular interactions in living cells than currently available FRET imaging methods.

Results and Discussion

Properties of the Selective Terbium Protein Label. We recently reported a method to impart terbium luminescence to recombinant fusion proteins (32). Heterodimeric conjugates of the common antibiotic trimethoprim (TMP) covalently linked to various terbium chelates were developed that bind noncovalently to eDHFR. TMP and eDHFR interact exclusively with one another in mammalian systems, and this interaction has been previously exploited to develop TMP-fluorophore conjugates that specifically label eDHFR fusion proteins in a variety of wild-type mammalian cell lines (LigandLink™ Universal Labeling Technology, Active Motif, Inc.) (33–35). In our previous study, we found that one particular conjugate, TMP-Lumi4 (Fig. 2*A*), bound tightly (K_D = ~2 nM) to a GFP-eDHFR fusion protein and that intramolecular terbium-to-GFP LRET could be detected with >100-fold dynamic range as long-lifetime, sensitized GFP emission in a cell-free assay (32).

The effectiveness of TMP-Lumi4 as a LRET donor to GFP results from its overall brightness, long lifetime, and the ability to spectrally discriminate GFP emission from terbium emission. Lumi4®-Tb is an exceptionally bright ($\varepsilon \approx 26{,}000\ M^{-1}\,cm^{-1}$ at

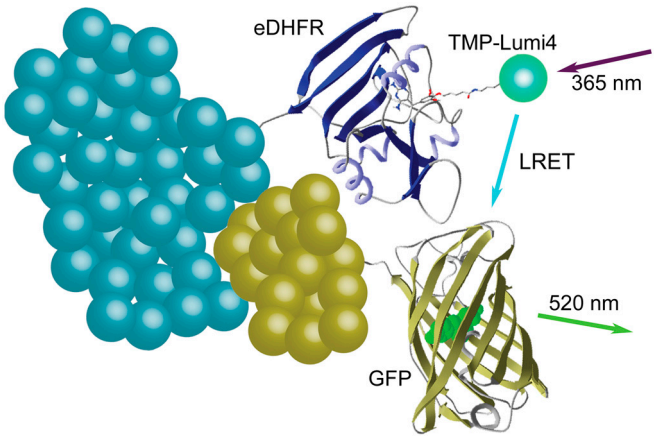

Fig. 1. Schematic representation of intermolecular terbium-to-GFP LRET. TMP-Lumi4 binds specifically and tightly to eDHFR (K_D = ~2 nM). Interaction between eDHFR and GFP fusion proteins and excitation of TMP-Lumi4 (the donor) results in LRET-sensitized emission of GFP (the acceptor). Time-resolved microscopy detects long-lifetime, sensitized GFP emission while eliminating cellular autofluorescence and directly excited GFP fluorescence background signals.

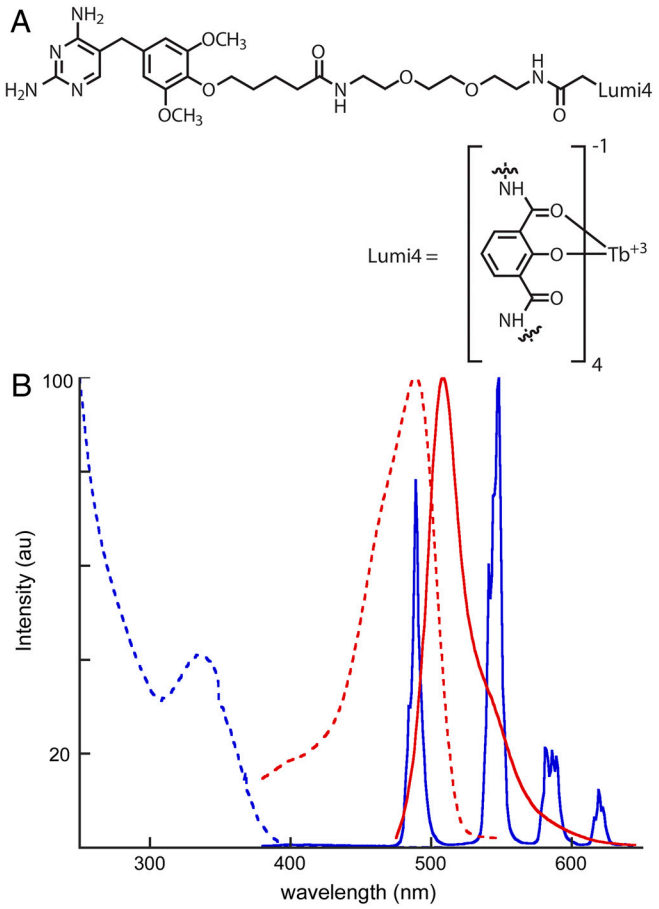

Fig. 2. (*A*) Structure of TMP-Lumi4, a conjugate of trimethoprim covalently linked to a proprietary analog of a multidentate 2-hydroxyisophthalamide terbium chelate (Lumi4®-Tb) (36). The molecule has a molecular weight of 1879 and a net charge of −1 when complexed with terbium. (*B*) Normalized absorption (dotted) and emission (solid) spectra of TMP-Lumi4 (blue) and EGFP (red). The characteristically narrow terbium emission bands enable efficient spectral separation of signals.

354 nm, quantum yield = 0.59) and long-lived ($\tau \approx 2.7$ ms) proprietary analog of a multidentate 2-hydroxyisophthalamide terbium chelate previously reported by Raymond and coworkers (36). TMP-Lumi4 exhibits characteristic terbium luminescence upon excitation with near-UV light and absorbs strongly at 365 nm, enabling efficient excitation with commercially available light-emitting diode (LED) sources (Fig. 2*B*). Both TMP-Lumi4 and unconjugated Lumi4®-Tb were found to exhibit single-exponential decay kinetics with the same apparent lifetime (~2.3 ms) under identical experimental conditions (Fig. S1). Terbium-sensitized GFP emission from a complex of TMP-Lumi4 bound to GFP-eDHFR occurred with single-exponential kinetics and an apparent lifetime of ~0.8 ms (Fig. S1). From lifetime data, we calculated an efficiency of ~67% for energy transfer from terbium to GFP in the TMP-Lumi4/GFP-eDHFR complex (*SI Materials and Methods*).

Intracellular Probe Delivery and Specific Protein Labeling. TMP-Lumi4 will not diffuse passively into cells from culture medium (32). Therefore, to perform intracellular LRET imaging, it was first necessary to establish methods of cytoplasmic probe delivery. Microinjection is one possible approach for loading adherent cells, and it has been successfully used for lanthanide complex delivery (25). However, microinjection requires specialized apparatus and can only be used to load relatively few cells at a time. Two techniques were therefore adapted to simultaneously deliver TMP-Lumi4 to the cytoplasm of many cells: (*i*) reversible plasma membrane permeabilization with streptolysin O (SLO) (37); and (*ii*) osmotic lysis of pinocytic vesicles (38, 39). Both methods consistently yielded >50% loading efficiency while maintaining ~95% cell viability 2 h posttreatment (Table S1).

Whereas both loading techniques have negligible effects on cell viability, the pinocytosis method should be less perturbative to cellular physiology, as the cell membrane is not compromised at any point during the process. With the pinocytic loading method, cells are allowed to undergo pinocytosis in a hypertonic medium containing sucrose, polyethylene glycol, and TMP-Lumi4. Upon transfer to a hypotonic medium, the pinocytic vesicles (containing TMP-Lumi4) burst due to the lowering of osmotic pressure, releasing their contents into the cytoplasm. The overall amount of TMP-Lumi4 delivered into cells can be controlled by varying the concentration in the hypertonic loading medium, or alternatively, by repeated applications of the pinocytosis/lysis process. Given a natural rate of pinocytosis equaling $\sim 10^{-16}$ L/min for most cell types (39), and assuming typical cell volumes of $\sim 10^{-12}$ L, the estimated cellular concentration of TMP-Lumi4 was $< 10^{-7}$ M for the experimental conditions used in this study (single loading application, 50 μM TMP-Lumi4, 10 min. pinocytosis) (*SI Materials and Methods*).

Intracellular delivery of TMP-Lumi4 and specific labeling of eDHFR fusion proteins was visualized using time-resolved microscopy. A conventional epifluorescence microscope was adapted for time-resolved imaging by incorporating a fast-modulated, UV LED ($\lambda_{em} = 365$ nm) as the excitation source and an intensified CCD camera for image acquisition. The LED circuitry allowed for either continuous wave emission or external on/off modulation with ~1 μs time resolution. The excitation intensity could be varied; however, we held the intensity constant at a measured value of 1.6 mW at the objective back aperture, yielding an estimated illumination intensity of ~0.6 W/cm^2 at the image plane (see *SI Materials and Methods*). The image intensifier component of the camera served as both a fast shutter and emission signal amplifier. By synchronizing the LED and intensifier with a digital delay generator, the excitation pulse width, the gate delay (time between pulse and detection), the gate width (intensifier on-time), and the pulse/detection repetition rate could be varied independently. The output from multiple excitation/detection cycles could be integrated on the CCD during a single camera frame, and the camera control software allowed summation of multiple frames (see *SI Materials and Methods* and Table S2 for microscope operation parameters used in this study).

Madin Darby Canine kidney (MDCKII) epithelial cells were transiently cotransfected with two plasmid DNA vectors; one that expressed nucleus-localized eDHFR and another that expressed nucleus-localized CFP as a positive control for transfection. After SLO-mediated delivery of TMP-Lumi4, a time-resolved image (gate delay = 10 μs) of broadband emission (>400 nm) revealed specific localization of terbium luminescence in the nucleus of a transfected cell loaded with probe (Fig. 3*A*). When unconjugated TMP (final conc. ~ 10 μM) was added to the imaging medium, it diffused into cells, competed with TMP-Lumi4 for eDHFR binding, and markedly diminished nuclear luminescence (Fig. 3*A*). Specific labeling of nucleus-localized eDHFR was also observed in NIH3T3 fibroblast cells that were loaded with TMP-Lumi4 by SLO-mediated membrane permeabilization (Fig. S2), and results seen with pinocytic delivery were similar.

Cytoplasmic delivery of TMP-Lumi4 and specific labeling of eDHFR was further assessed by imaging terbium-to-GFP LRET in time-resolved mode. MDCKII cells were transfected with DNA encoding a GFP-eDHFR fusion protein. The cells were loaded with TMP-Lumi4 by pinocytic delivery, and intramolecu-

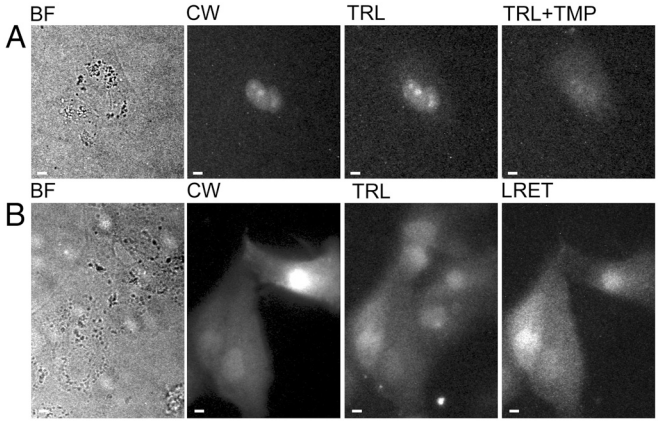

Fig. 3. Both streptolysin O (SLO)-mediated membrane permeabilization and osmotic lysis of pinocytic vesicles deliver TMP-Lumi4 to the cytoplasm of MDCKII cells, and specific labeling of eDHFR fusion proteins can be visualized by time-resolved luminescence microscopy. (*A*), (*B*) Micrographs: BF, bright field; CW, continuous wave fluorescence ($\lambda_{ex} = 480 \pm 20$ nm, $\lambda_{em} = 535 \pm 25$ nm); TRL, time-resolved luminescence ($\lambda_{ex} = 365$ nm, $\lambda_{em} > 400$ nm, gate delay = 10 μs); TRL + TMP, 20 min after addition of TMP (final conc. = 10 μM) to culture medium; LRET, time-resolved luminescence ($\lambda_{ex} = 365$ nm, $\lambda_{em} = 520 \pm 10$ nm, gate delay = 10 μs). TRL and TRL + TMP images were adjusted to identical contrast levels. Complete details of time-resolved microscopy parameters are provided in *SI Materials and Methods* and Table S2. Scale bars, 10 μm. (*A*) MDCKII cells transiently cotransfected with DNA encoding nucleus-localized CFP and nucleus-localized eDHFR were incubated with TMP-Lumi4 (15 μM) and streptolysin O (SLO, 50 ng/mL) for 10 min. Time-resolved detection of broadband (>400 nm) terbium emission reveals localization of TMP-Lumi4 in nucleus of transfected cell (corresponding to continuous wave fluorescence image of CFP emission). A time-resolved image taken 20 min. after addition of TMP (final conc. = 10 μM) to the culture medium shows diminished nuclear luminescence because TMP out-competes TMP-Lumi4 for binding to eDHFR. (*B*) MDCKII cells transiently transfected with DNA encoding GFP-eDHFR. Cells were incubated in hypertonic medium containing TMP-Lumi4 (50 μM) for 10 min to allow pinocytosis and subsequently exposed to hypotonic medium to effect lysis of pinocytic vesicles and release of probe into the cytoplasm. Time-resolved detection of broadband emission (>400 nm) reveals terbium luminescence in TMP-Lumi4-loaded cells. Luminescence resonance energy transfer (LRET) is seen only in transfected cells (indicated in continuous wave fluorescence image) coincidentally loaded with TMP-Lumi4 when visualized in time-resolved mode through a narrow-pass filter (520 ± 10 nm), indicating specific labeling of the GFP-eDHFR fusion protein.

lar, terbium-sensitized GFP emission was seen only in GFP-eDHFR-expressing cells when visualized in time-resolved mode through a narrow-pass filter ($\lambda_{em} = 520 \pm 10$ nm) that blocked terbium emission (Fig. 3*B*). Intramolecular, terbium-to-GFP LRET was also observed in NIH3T3 fibroblasts that were pinocytically loaded with TMP-Lumi4 (Fig. S2). These results and those above show that both SLO-mediated membrane permeabilization and osmotic lysis of pinocytic vesicles can effectively deliver TMP-Lumi4 into the cytoplasm of at least two cell types (MDCKII and NIH3T3). Upon cellular delivery, TMP-Lumi4 diffuses freely throughout the cytoplasm and nucleus without detectable nonspecific binding and binds selectively to eDHFR, suggesting that other methods of cytoplasmic delivery should prove equally useful. Moreover, time-resolved microscopy can visualize intramolecular terbium-to-GFP LRET as long-lifetime (>10 μs), sensitized GFP emission.

Quantification of LRET signals. The concentration of GFP-eDHFR or other fusion proteins expressed from a strong promoter (1–10 μM) (40) likely exceeds the estimated concentration of TMP-Lumi4 (<100 nM) in pinocytically loaded cells. Given its high affinity for eDHFR ($K_D = \sim 2$ nM), TMP-Lumi4 was assumed to be mostly bound to fusion protein, and therefore the LRET signal should vary with the amount of TMP-Lumi4 in the cell. To quantify the LRET signal, two time-resolved images were obtained using identical acquisition settings but for different emission wavelengths: (*i*) the pure sensitized GFP emission signal ($\lambda_{em} = 520 \pm 10$ nm); and (*ii*) a signal comprising terbium emission plus sensitized GFP emission ($\lambda_{em} = 540 \pm 10$ nm). For each cell in an image, the background-subtracted mean gray value was used as an indicator of emission intensity (*SI Materials and Methods* and Fig. S3). From these pairs of images, a donor-normalized LRET signal (LRETN) could then be calculated as the 520/540 emission ratio for each measured cell.

TMP-Lumi4 Stability and Photoresistance in cells. To be useful as cellular imaging probes, lanthanide complexes must remain stably luminescent in cells over time and must also be resistant to photobleaching. Long-term cellular stability may be compromised by endogenous chelators that could remove metal from the complex, rendering it nonluminescent. The stability of TMP-Lumi4 in MDCKII cells expressing GFP-eDHFR was determined by imaging terbium-to-GFP LRET. LRETN was observed to be constant over ~23 h (Fig. S4). However, the unnormalized LRET signal decreased approximately 50% over the same time period, from an initial value of 230 ± 100 to a value of 110 ± 65 at 23 h (mean ± s.d., >10-cell samples). The results suggest that TMP-Lumi4 remains stably luminescent within cells but may slowly leak out of the cells over time, and therefore the LRET signal remains quantitatively useful over the time course of the experiment.

The photoresistance of TMP-Lumi4 in MDCKII cells expressing GFP-eDHFR was determined by monitoring the LRET signal as a function of accumulated irradiation time. A field of view was exposed to continuous wave LED excitation at the standard illumination intensity (~0.6 W/cm^2). The LRET signal ($\lambda_{em} = 520 \pm 10$ nm) was measured on a cell-by-cell basis at successive timepoints, normalized to each cell's initial intensity, and fit to a single exponential decay, yielding an estimated photobleaching lifetime of ~2.0 min (Fig. S4). The measured photobleaching lifetime is considerably longer than typical image exposure times (seconds), and therefore time-lapse LRET imaging should be possible without concern for loss of signal due to photobleaching of the donor.

LRET Imaging of Protein–Protein Interactions. The ability of this unique LRET system to image protein–protein interactions was next used to measure the association of a PDZ domain with a carboxyl-terminal binding motif in living cells (41, 42). Such PDZ-mediated interactions are fundamental to biological function in species from Drosophila to mammals. In epithelia, a direct, high-affinity ($K_D = \sim 10$–20 nM) interaction between the C-terminal cytoplasmic tail of claudin-1 and the most N-terminal PDZ domains (PDZ1) of ZO-1 and the related proteins ZO-2 and ZO-3 has been demonstrated using isolated recombinant proteins (43). Moreover, PDZ1 domains of ZO-1, ZO-2, and ZO-3 are recruited to sites of claudin-1 polymerization in transfected fibroblasts (43) but not to sites enriched in mutant claudin-1 lacking the C-terminal YV motif (43). The relevance of this interaction to disease is emphasized by the observations that mutations within the ZO-2 PDZ1 domain are linked to familial hypercholanemia (44), a disease of hepatic bile transport, whereas loss of claudin-1 expression is associated with neonatal sclerosing cholangitis (45), another hereditary cholestatic disease. However, a direct interaction between the C-terminal claudin-1 YV motif and the first PDZ domain of ZO-1 has not been previously demonstrated in live cells.

To examine the interaction between claudin-1 and ZO-1 in living cells, MDCKII cells were transfected with expression vectors encoding a C-terminal fusion of eDHFR to the PDZ1 domain (residues 19–113) of ZO-1 (ZO-1/PDZ1-eDHFR) and an N-terminal fusion of EGFP to the C-terminal cytoplasmic domain (residues 187–211) of claudin-1 (GFP-cldn1/tail). Transfected cells were loaded with TMP-Lumi4 using both SLO-mediated and pinocytic delivery methods. In both cases, LRET imaging revealed terbium-sensitized GFP emission only in transfected cells loaded with TMP-Lumi4, providing an unambiguous image of protein–protein interaction (Fig. 4*A* and Fig. S2). The LRETN for pinocytically loaded cells equaled 0.38 ± 0.10 (mean ± s.d., Table S3). Addition of excess TMP to growth med-

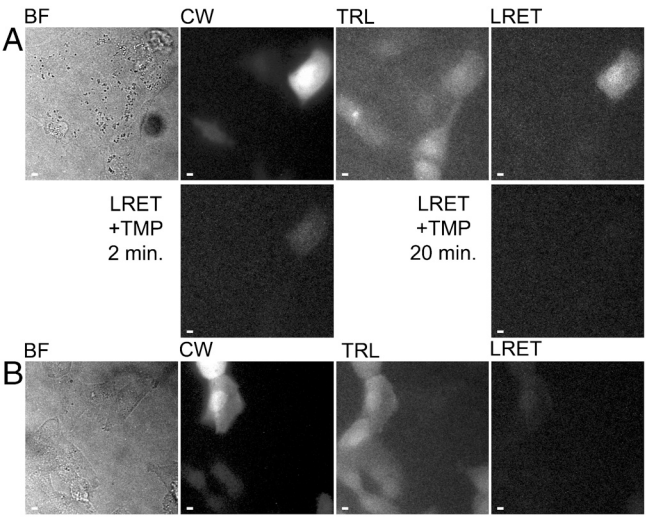

Fig. 4. Time-resolved LRET imaging reveals interaction between ZO-1/PDZ1-eDHFR and GFP-cldn1/tail in MDCKII cells. (*A*), (*B*) Micrographs: BF, bright field; CW, continuous wave fluorescence ($\lambda_{ex} = 480 \pm 20$ nm, $\lambda_{em} = 535 \pm 25$ nm); TRL, time-resolved luminescence ($\lambda_{ex} = 365$ nm, $\lambda_{em} > 400$ nm, gate delay = 10 μs); LRET, time-resolved luminescence ($\lambda_{ex} = 365$ nm, $\lambda_{em} = 520 \pm 10$ nm, gate delay = 10 μs); LRET + TMP, after addition of TMP (final conc. = 10 μM) to growth medium at indicated time-points. LRET and LRET + TMP images were adjusted to identical contrast levels. Complete details of time-resolved microscopy parameters are provided in *SI Materials and Methods* and Table S2. Scale bars, 10 μm. (*A*) MDCKII cells coexpressing ZO-1/PDZ1-eDHFR and GFP-cldn1/tail loaded with TMP-Lumi4 by osmotic lysis of pinosomes. Terbium-to-GFP LRET is seen only in transfected cells loaded with TMP-Lumi4. When TMP is added to culture medium, it displaces TMP-Lumi4 from the ZO-1/PDZ1-eDHFR/GFP-cldn1/tail complex, eliminating the LRET signal. (*B*) MDCKII cells coexpressing ZO-1/PDZ1-eDHFR and GFP-cldn1/tail$^{\Delta YV}$, loaded with TMP-Lumi4 as in (*A*). No LRET signal is seen in expressing cells loaded with TMP-Lumi4.

ium eliminated the LRET signal (Fig. 4*A*), further confirming that long-lifetime, sensitized GFP emission results from specific binding of TMP-Lumi4 to ZO-1/PDZ1-eDHFR. The predominantly nuclear localization of interactions between ZO-1/PDZ1-eDHFR and the GFP-cldn1/tail is consistent with previous reports showing that GFP-tagged ZO-1 PDZ1 domain accumulates within the nucleus (43) and that ZO-1 directs subcellular claudin trafficking (46).

To assess specificity of the observed interaction, a GFP-cldn1/tail construct lacking the C-terminal YV motif (GFP-cldn1/tail$^{\Delta YV}$) was developed and expressed in MDCKII cells with ZO-1/PDZ1-eDHFR. Whereas continuous widefield GFP fluorescence and broadband, time-resolved terbium luminescence signals were easily detected in cells loaded with TMP-Lumi4, only extremely faint LRET was seen (Fig. 4*B*), verifying that the LRET signal observed between ZO-1/PDZ1-eDHFR and GFP-cldn1/tail reflects a specific PDZ-mediated interaction. There was a highly significant ($P < 10^{-6}$), >6-fold difference between the mean LRETN signal from cells expressing ZO-1/PDZ1-eDHFR and GFP-cldn1/tail (0.38 ± 0.10) and that seen from cells expressing ZO-1/PDZ1-eDHFR and GFP-cldn1/tail$^{\Delta YV}$ (0.06 ± 0.04, mean $\pm$ s.d., Table S3).

The data above show that LRET imaging is faster, more sensitive, and in many respects, less complex than widefield, steady-state FRET microscopy. With steady-state FRET, the sensitized emission signal is contaminated by directly excited donor and acceptor fluorescence. Therefore, multiple control images must be collected, requiring acquisition times of at least ~3 s on optimized systems (12, 16, 17). Even with careful image acquisition and proper analysis, signal changes of only ~10% are typically observed between FRET-positive samples and negative controls (14, 15). By contrast, LRET imaging only detects signals emanating from interacting molecules. We observed a ~500% increase in mean LRETN between cells expressing interacting and noninteracting ZO-1/PDZ1-eDHFR and GFP-cldn1/tail pairs (Table S3), and this result represents a ~50-fold increase in signal-to-background ratio over that typically observed with steady-state FRET imaging of protein–protein interactions.

The dramatic difference in measured signal between LRET-positive cells and negative controls is partly due to the high affinity between ZO-1/PDZ1 and cldn1/tail (in vitro $K_D = 13$ nm) (45). The high affinity makes it likely that most of the TMP-Lumi4 delivered into cells was bound to ZO-1/PDZ1-eDHFR and donated energy to proximal GFP-cldn1/tail. Measurements of lower-affinity interactions should be possible using the LRET method, however, longer image acquisition times may be necessary to generate sufficient signal. Alternatively, increased loading of TMP-Lumi4 (up to saturation of eDHFR binding) would yield a higher measured signal level. For LRETN calculations, we used images that were acquired at relatively long acquisition times (8 s, Table S2), although intermolecular LRET could be detected with acquisition times as short as 0.67 s (Fig. S5). Thus, in addition to enhanced sensitivity, LRET imaging displays increased time resolution that may allow analysis of interaction dynamics that cannot be resolved by traditional steady-state FRET or FRET-FLIM. Whereas other optical methodologies such as induced translocation of fluorescent protein fusions (7–9) and FCCS (4, 5) can monitor interactions in cells with much better time resolution (0.1–1 s for FCCS), these methods do not provide a spatial map of interactions.

Conclusion

Our results show that eDHFR fusion proteins can be specifically and stably labeled with a luminescent terbium complex, TMP-Lumi4, in living, wild-type mammalian cells. The ability to selectively impart terbium luminescence enables dynamic, nondestructive LRET imaging of intracellular interactions between eDHFR and GFP fusion proteins without additional control measurements and mathematical processing. By detecting terbium-sensitized GFP emission at long lifetimes, we effectively eliminate detection of cellular autofluorescence, unbound terbium probe luminescence, and directly excited GFP fluorescence, thereby imaging LRET in living cells at time scales (<1 s) that are substantially faster than steady-state FRET imaging (~3 s) and orders of magnitude faster than FLIM imaging of FPs.

Whereas the techniques described here should improve live-cell studies of protein function, there is broad scope for further enhancements and modifications. For instance, intramolecular LRET could be exploited to develop biosensors that incorporate eDHFR and GFP in a single fusion protein, analogous to CFP/YFP sensors designed to detect cellular analytes or enzyme activity (13). Time-resolved microscopy can also be adapted to measure donor or sensitized acceptor lifetimes by capturing and analyzing a series of images at different detector delay intervals (47, 48). The multiple terbium emission peaks of TMP-Lumi4 can serve as a LRET donor to both GFP and red fluorescent proteins, potentially enabling the simultaneous detection of more than one molecular interaction in a single living cell (Fig. 2*B*). Finally, both SLO and pinocytosis probe delivery methods can be easily adapted for use in multiwell plate format, enabling high-throughput screening assays of intracellular protein–protein interactions using commercially available time-resolved fluorescence plate readers.

Materials and Methods

Chemical Synthesis. Details describing the synthesis and characterization of TMP-Lumi4 can be found in *SI Materials and Methods* and in Rajapakse et al. (32).

Cell Culture, Transfection, and Probe Delivery Methods. NIH3T3 and MDCKII cells were cultured and and transfected with plasmid DNA according to standard protocols. Complete details of these as well as methods for pinocytic and SLO-mediated probe delivery and cell viability assay protocols are provided in *SI Materials and Methods*.

Live Cell Imaging and Data Analysis. Comprehensive descriptions of the time-resolved microscope system, image acquisition parameters and methods of image processing and data analysis are offered in *SI Materials and Methods*.

ACKNOWLEDGMENTS. We thank K.N. Raymond (University of California) and N.G. Butlin (Lumiphore, Inc.) for material and intellectual support. Lumi4®-Tb is a registered trademark of Lumiphore, Inc. We thank V.W. Cornish (Columbia University) for providing GFP-eDHFR plasmid. This study was supported by the National Institutes of Health (National Institute of General Medical Sciences Grant R01GM081030 and National Institute of Diabetes and Digestive and Kidney Diseases Grant R01DK061931) and by the Chicago Biomedical Consortium (C-008, with support from The Searle Funds at The Chicago Community Trust).

1. Pawson T, Nash P (2003) Assembly of cell regulatory systems through protein interaction domains. *Science* 300(5618):445–452.
2. Fields S, Song O (1989) A novel genetic system to detect protein–protein interactions. *Nature* 340(6230):245–246.
3. Phizicky EM, Fields S (1995) Protein–protein interactions: Methods for detection and analysis. *Microbiol Rev* 59(1):94–123.
4. Baudendistel N, Muller G, Waldeck W, Angel P, Langowski J (2005) Two-hybrid fluorescence cross-correlation spectroscopy detects protein–protein interactions in vivo. *Chemphyschem* 6(5):984–990.
5. Kim SA, Heinze KG, Waxham MN, Schwille P (2004) Intracellular calmodulin availability accessed with two-photon cross-correlation. *Proc Natl Acad Sci USA* 101(1):105–110.
6. Kerppola TK (2006) Visualization of molecular interactions by fluorescence complementation. *Nat Rev Mol Cell Biol* 7(6):449–456.
7. Heydorn A, Lundholt BK, Praestegaard M, Pagliaro L (2006) Protein translocation assays: Key tools for accessing new biological information with high-throughput microscopy. *Methods Enzymol* 414:513–530.
8. Knauer SK, Stauber RH (2005) Development of an autofluorescent translocation biosensor system to investigate protein–protein interactions in living cells. *Anal Chem* 77(15):4815–4820.
9. Piljic A, Schultz C (2008) Analysis of protein complex hierarchy in living cells. *ACS Chem Biol* 3(12):749–755.
10. Jares-Erijman EA, Jovin TM (2003) FRET imaging. *Nat Biotechnol* 21(11):1387–1395.

11. Piston DW, Kremers GJ (2007) Fluorescent protein FRET: The good, the bad, and the ugly. *Trends Biochem Sci* 32(9):407–414.
12. Vogel SS, Thaler C, Koushik SV (2006) Fanciful FRET. *Sci STKE*(331):re2.
13. Zhang J, Campbell RE, Ting AY, Tsien RY (2002) Creating new fluorescent probes for cell biology. *Nat Rev Mol Cell Biol* 3(12):906–918.
14. Kunkel MT, Garcia EL, Kajimoto T, Hall RA, Newton AC (2009) The protein scaffold NHERF-1 controls the amplitude and duration of localized protein kinase D activity. *J Biol Chem* 284(36):24653–24661.
15. Llopis J, et al. (2000) Ligand-dependent interactions of coactivators steroid receptor coactivator-1 and peroxisome proliferator-activated receptor binding protein with nuclear hormone receptors can be imaged in live cells and are required for transcription. *Proc Natl Acad Sci USA* 97(8):4363–4368.
16. Berney C, Danuser G (2003) FRET or no FRET: A quantitative comparison. *Biophys J* 84(6):3992–4010.
17. Gordon GW, Berry G, Liang XH, Levine B, Herman B (1998) Quantitative fluorescence resonance energy transfer measurements using fluorescence microscopy. *Biophys J* 74(5):2702–2713.
18. Nguyen AW, Daugherty PS (2005) Evolutionary optimization of fluorescent proteins for intracellular FRET. *Nat Biotechnol* 23(3):355–360.
19. Mathis G (1993) Rare earth cryptates and homogeneous fluoroimmunoassays with human sera. *Clin Chem* 39(9):1953–1959.
20. Prat O, Lopez E, Mathis G (1991) Europium(III) cryptate: A fluorescent label for the detection of DNA hybrids on solid support. *Anal Biochem* 195(2):283–289.
21. Selvin PR (2002) Principles and biophysical applications of lanthanide-based probes. *Annu Rev Biophys Biomol Struct* 31:275–302.
22. Selvin PR, Hearst JE (1994) Luminescence energy transfer using a terbium chelate: Improvements on fluorescence energy transfer. *Proc Natl Acad Sci USA* 91(21): 10024–10028.
23. Leblanc V, et al. (2002) Homogeneous time-resolved fluorescence assay for identifying p53 interactions with its protein partners, directly in a cellular extract. *Anal Biochem* 308(2):247–254.
24. Maurel D, et al. (2008) Cell-surface protein–protein interaction analysis with time-resolved FRET and snap-tag technologies: Application to GPCR oligomerization. *Nat Methods* 5(6):561–567.
25. Hanaoka K, Kikuchi K, Kobayashi S, Nagano T (2007) Time-resolved long-lived luminescence imaging method employing luminescent lanthanide probes with a new microscopy system. *J Am Chem Soc* 129(44):13502–13509.
26. Law GL, et al. (2008) Emissive terbium probe for multiphoton in vitro cell imaging. *J Am Chem Soc* 130(12):3714–3715.
27. Montgomery CP, Murray BS, New EJ, Pal R, Parker D (2009) Cell-penetrating metal complex optical probes: Targeted and responsive systems based on lanthanide luminescence. *Acc Chem Res* 42(7):925–937.
28. Song B, Vandevyver CD, Chauvin AS, Bunzli JC (2008) Time-resolved luminescence microscopy of bimetallic lanthanide helicates in living cells. *Org Biomol Chem* 6(22): 4125–4133.
29. Botchway SW, et al. (2008) Time-resolved and two-photon emission imaging microscopy of live cells with inert platinum complexes. *Proc Natl Acad Sci USA* 105(42):16071–16076.
30. de Haas RR, et al. (1999) Phosphorescent platinum/palladium coproporphyrins for time-resolved luminescence microscopy. *J Histochem Cytochem* 47(2):183–196.
31. de Haas RR, et al. (1997) Platinum porphyrins as phosphorescent label for time-resolved microscopy. *J Histochem Cytochem* 45(9):1279–1292.
32. Rajapakse HE, Reddy DR, Mohandessi S, Butlin NG, Miller LW (2009) Luminescent terbium protein labels for time-resolved microscopy and screening. *Angew Chem Int Ed Engl* 48(27):4990–4992.
33. Calloway NT, et al. (2007) Optimized fluorescent trimethoprim derivatives for in vivo protein labeling. *Chembiochem* 8(7):767–774.
34. Gallagher SS, Sable JE, Sheetz MP, Cornish VW (2009) An in vivo covalent TMP-tag based on proximity-induced reactivity. *ACS Chem Biol* 4(7):547–556.
35. Miller LW, Cai Y, Sheetz MP, Cornish VW (2005) In vivo protein labeling with trimethoprim conjugates: A flexible chemical tag. *Nat Methods* 2(4):255–257.
36. Petoud S, Cohen SM, Bunzli JC, Raymond KN (2003) Stable lanthanide luminescence agents highly emissive in aqueous solution: multidentate 2-hydroxyisophthalamide complexes of $Sm(3+)$, $Eu(3+)$, $Tb(3+)$, $Dy(3+)$. *J Am Chem Soc* 125(44):13324–13325.
37. Ahnert-Hilger G, Bader MF, Bhakdi S, Gratzl M (1989) Introduction of macromolecules into bovine adrenal medullary chromaffin cells and rat pheochromocytoma cells (PC12) by permeabilization with streptolysin O: Inhibitory effect of tetanus toxin on catecholamine secretion. *J Neurochem* 52(6):1751–1758.
38. Okada CY, Rechsteiner M (1982) Introduction of macromolecules into cultured mammalian cells by osmotic lysis of pinocytic vesicles. *Cell* 29(1):33–41.
39. Rechsteiner M (1987) Osmotic lysis of pinosomes. *Methods Enzymol* 149:42–48.
40. Tsien RY (1998) The green fluorescent protein. *Annu Rev Biochem* 67:509–544.
41. Songyang Z, et al. (1997) Recognition of unique carboxyl-terminal motifs by distinct PDZ domains. *Science* 275(5296):73–77.
42. Doyle DA, et al. (1996) Crystal structures of a complexed and peptide-free membrane protein-binding domain: Molecular basis of peptide recognition by PDZ. *Cell* 85(7):1067–1076.
43. Itoh M, et al. (1999) Direct binding of three tight junction-associated MAGUKs, ZO-1, ZO-2, and ZO-3, with the COOH termini of claudins. *J Cell Biol* 147(6):1351–1363.
44. Carlton VE, et al. (2003) Complex inheritance of familial hypercholanemia with associated mutations in TJP2 and BAAT. *Nat Genet* 34(1):91–96.
45. Hadj-Rabia S, et al. (2004) Claudin-1 gene mutations in neonatal sclerosing cholangitis associated with ichthyosis: A tight junction disease. *Gastroenterology* 127(5):1386–1390.
46. Umeda K, et al. (2006) ZO-1 and ZO-2 independently determine where claudins are polymerized in tight-junction strand formation. *Cell* 126(4):741–754.
47. Elangovan M, Day RN, Periasamy A (2002) Nanosecond fluorescence resonance energy transfer-fluorescence lifetime imaging microscopy to localize the protein interactions in a single living cell. *J Microsc* 205(1):3–14.
48. Heyduk T, Heyduk E (2001) Luminescence energy transfer with lanthanide chelates: interpretation of sensitized acceptor decay amplitudes. *Anal Biochem* 289(1):60–67.

Supporting Information

Rajapakse et al. 10.1073/pnas.1002025107

SI Text

SI Materials and Methods. All chemicals were purchased from Sigma Aldrich. Lumi4®-NHS was a kind gift from Lumiphore, Inc. Purified GFP-eDHFR was prepared as described previously (1). Dulbecco's modified eagle medium (DMEM), Dulbecco's phosphate buffered saline (PBS), Hank's buffered salt solution (HBSS), fetal bovine serum, Lipofectamine™ 2000 transfection reagent, buffers and reagents for pinocytosis/osmotic lysis (Influx™ reagent, cat. no. I-14402), and reagents for cell viability testing (LiveDead™ assay, cat. no. L3224) were purchased from Invitrogen, Inc. Streptolysin O (SLO) was obtained from MBL International, Inc. Low-resolution electrospray (ESI) mass spectra were obtained at the UIC Research Resources Center (RRC). UV-Vis absorption spectra were recorded using a Cary 3000 spectrophotometer (Varian, Inc.). Fluorescence emission spectra were recorded using a Fluoromax 3 fluorimeter (Horiba–Jobin Yvon, Inc.). Reversed-phase HPLC was performed using a Beckman System Gold instrument equipped with an analytical scale pump (model 128), a UV-Vis detector (model 168) and a C18 analytical column (GraceVydac, cat. no. 218TP54, 5 μm, 4.6 mm i.d. × 250 mm).

Synthesis of TMP-lumi4®. A derivative of trimethoprim substituted with an amine-terminated, 15-atom linker at the 4′ position (TMP-NH2) was prepared as previously described (1). TMP-NH2 (2 μmol, 1.0 eqiv.) was dissolved in 1.0 mL dry DMF and *ca.* 1 uL of diisopropyl ethylamine (*ca.* 5 μmol, 2.5 eqiv.) under nitrogen atmosphere. An N-hydroxy succinimidyl derivative of Lumi4® (Lumi4®-NHS) was dissolved in 0.5 mL DMF (2 μmol, 1.0 equiv) and added to the reactants. The solution was stirred at room temperature under nitrogen for 18 h. Product was purified by HPLC using 20 min linear gradient, from 5% to 35% solvent B (solvent A, 0.1 M triethylammonium acetate (pH 6.5) plus 5% CH_3CN; solvent B, CH_3CN). The fractions containing the desired compound were pooled, rotary evaporated to remove CH_3CN, and lyophilized to yield the desired compound. ESI-MS^+ ($C_{85}H_{115}N_{19}O_{20}$): m/z 1722.87 $[M + H]^+$.

Metal labeling. A stock solution of TMP-Lumi4 (300 μM in H_2O) was prepared. Concentration was estimated by measuring absorption at 339 nm and an extinction coefficient of 26,000 M^{-1} cm^{-1}. Aliquots were labeled with terbium as needed by combining with ~1.2 equiv. $TbCl_3$ in 1.5 mL centrifuge tubes, vortexing ~5 min, and resting at RT for *ca.* 30 min. Dilutions of the terbium-labeled compound into appropriate assay buffers could then be made for requisite spectroscopy or microscopy experiments.

Cell culture and transfection. NIH 3T3 and MDCKII cells were cultured in Dulbecco's Modified Eagle Media (DMEM, Invitrogen) supplemented with 10% FBS, 2 mM L-glutamine, 100 unit/mL penicillin and 100 mg/mL of streptomycin at 37 °C and 5% CO_2. NIH 3T3 and MDCK cells were passaged using 0.05% trypsin/0.03% EDTA solution (GIBCO) and 0.25% trypsin/0.03% EDTA solution, respectively.

Plasmids. Plasmid pLM1301 (expressing nucleus-localized CFP) described previously (2). Plasmid pLL1-NLS (expressing nucleus-localized eDHFR) was obtained from Active Motif, Inc. A plasmid expressing a C-terminal fusion of eDHFR to EGFP under constitutive control of the cytomegalovirus promoter was provided by Prof. V.W. Cornish. GFP-cldn1/tail was created by cloning amino acids 187–211 of human claudin-1 into pEGFP-C1 (Clontech). GFP-cldn1/$tail^{\Delta YV}$ was generated by point mutation to create a premature stop codon. ZO-1/PDZ1-eDHFR was created by inserting amino acids 19–113 of human ZO-1 (preceded by a start codon) into pLL-1NLS in frame with eDHFR. The integrity of all plasmids was verified by direct sequencing.

Cell transfection. NIH3T3 or MDCKII cells were seeded at 10^5 cells per well into a 6-well plate. After ~18 h incubation at 37 °C and 5% CO_2, adherent cells (~80% confluent) were transfected with 2 μg of the desired plasmid DNA using Lipofectamine2000™ transfection reagent (Invitrogen) according to manufacturer's instructions. Approximately 6 h after transfection, cells were trypsinized and reseeded at 14,000 cells/well into 8-well chambered slides and incubated at 37 °C and 5% CO_2 overnight.

Probe delivery via osmotic lysis of pinosomes. A 6 μL aliquot of TMP-Lumi4 (300 μM in H_2O) was combined with ~1.2 equivalents of $TbCl_3$ (in ~3 μL H_2O), vortexed for 5 min., and allowed to stand at room temperature for 30 min. This step effects chelation of terbium, rendering the probe luminescent. The metal-labeled TMP-Lumi4 solution (~9 μL) was combined with 27 μL of hypertonic growth medium (Influx™ reagent, Invitrogen, prepared according to manufacturer's instruction). NIH3T3 or MDCKII cells in a single well of an 8-well chambered slide were washed 1× with prewarmed (37º C) PBS and2× with prewarmed hypertonic solution, respectively. Then, prewarmed hypertonic solution containing TMP-Lumi4 was added, and the cells were incubated at 37 °C and 5% CO_2 for exactly 10 min. The cells were then quickly washed 2× with hypotonic solution (Influx™ reagent, Invitrogen, prepared according to manufacturer's instruction) and allowed to incubate in hypotonic solution for exactly 2 min. at room temperature to effect lysis of pinosomes. The cells were then washed 2× with PBS, immersed in complete DMEM and incubated for ~1 h at 37 °C and 5% CO_2 before imaging.

Probe delivery via streptolysin O (SLO)-mediated membrane permeabilization. SLO (1 mg/mL in PBS/50% glycerol, MBL International, Inc.) was diluted to a final concentration of 1000 ng/mL in 10 mM DTT/PBS and incubated at 37 °C for 2 h. The preactivated SLO was aliquoted and stored at −20 °C for later use. In a typical experiment, terbium-chelated TMP-Lumi4 was diluted to 15 μM in 100 μL Hank's buffered salt solution (HBSS). Preactivated SLO was added to a final concentration of 50 ng/mL (1:20 dilution of preactivated SLO stock solution). NIH3T3 or MDCKII cells in a single well of an 8-well chambered slide were washed 3× with prewarmed (37 °C) HBSS. Then, 150 μL of prewarmed TMP- Lumi4/SLO/HBSS solution was added, and the cells were incubated at 37 °C and 5% CO_2 for exactly 10 min. After incubation, 300 μL of DMEM containing 1.8 mM Ca^{2+} was added to the cells to effect resealing of membranes. The cells were incubated for at least 1 h at 37 °C and 5% CO_2 before washing 3× w/PBS and immersion in DMEM prior to imaging.

Cell viability assay. A standard assay for cell viability (Live-dead™ assay, Invitrogen, Inc., L3224) was used to assess the effects of SLO and osmotic lysis of pinosomes on MDCKII and NIH3T3 cells. Three separate experiments were performed for each cell type/treatment protocol, and the total number of living and dead

cells was summed. Greater than 93% of cells are alive 2 h after treatment ($n > 600$ for each condition, Table S1).

Live cell imaging. Microscopy of adherent live cells was performed using an epifluorescence microscope (Zeiss Axiovert 200) modified with the following components: (*i*) a fast-modulated UV LED emitting at 365 nm (UV-LED-365, Prizmatix, Ltd.); (*ii*) delay generator (DG645, Stanford Research Systems, Inc.); (*iii*) a gated image-intensified CCD camera (ICCD, mounted on the side-port of the microscope) and camera controller (Mega-10EX, Stanford Photonics, Inc.); and (*iv*) a computer running Piper Control software (v2.4.05, Stanford Photonics, Inc.). A 100 W mercury arc lamp was available for continuous wave fluorescence excitation, and a conventional CCD (Zeiss Axiocam MRM) was mounted on the front port of the microscope. Filter cubes containing the appropriate excitation and emission filters and dichroics allowed for wavelength selection. Samples were imaged with a 63X/1.25 N.A. EC Plan Neofluar oil-immersion objective (Carl Zeiss, Inc.) For continuous-wave fluorescence and bright field images, the ICCD was set to "Live" mode, with automatic gain level and acquisition time.

The UV LED excitation source provides a collimated output that we measured to equal ~50 mW at the exit window. The LED circuitry allows for continuous wave emission or external TTL modulation with submicrosecond rise/fall times. The excitation intensity could be varied, however, we held the intensity constant at a measured value of 1.6 mW at the objective back aperture. Using the method of Grünwald, et al. (3) we estimated the illumination intensity to equal ~0.6 W/cm^2 at the image plane when using the Zeiss EC Plan Neofluar 63× 1.25 N.A. objective.

For time-resolved microscopy with pulsed, near-UV excitation, image acquisition was initiated by a start signal (TTL) from the computer to the delay generator. Separate outputs (TTL) routed from the delay generator to the UV LED and the ICCD (via the camera controller) relayed a preprogrammed "burst" sequence to trigger the LED and the intensifier a user-defined number of times. For each acquisition, the signal from multiple excitation/emission events was accumulated on the ICCD sensor and read out to the image capture card of the computer at the end of the camera frame. The UV LED pulse width and pulse period, the intensifier delay time and on-time, the camera frame length (66.67 ms–2 s) and the intensifier gain voltage could be varied independently.

The source/camera timing parameters were the same for all of the time-resolved images and data presented here: excitation pulse width = 1500 μs, pulse period = 3000 μs, delay time = 10 μs, intensifier on-time = 1390 μs. The sensitivity of the time-resolved microscope is partly dependent on the number of excitation/detection events integrated on the CCD during a single camera frame and on the intensifier gain voltage. The signal-to-noise ratio, and thus the precision with which time-resolved data can be acquired is improved by summing multiple frames to generate a single image (at the expense of longer image acquisition times). Each frame summed effectively increases the bit depth of the resulting image by a factor of 1024 (i.e., 1 frame yields bit depth equal to 1024, 2 frames, 2048, etc.). A feature of the camera control software was enabled that removes large variations in signal resulting from ion-feedback noise of the intensifier. Table S2 lists the number of excitation/detection events, frame length, number of frames, total acquisition time and intensifier gain voltage used to acquire all time-resolved images and/or datasets reported in the paper and in *SI Text*.

Image processing and data analysis. Images (tagged image file format, .TIF) were captured with Piper control software (v2.4.05, Stanford Photonics, Inc.). and rendered using NIH Image J (v1.34). Micrographs showing LRET images and their associated controls were presented with identical contrast levels. Table S2 provides the image processing parameters applied to each time-resolved image in the paper, including pixel dimensions, pixel (bit) depth and contrast level (minimum and maximum gray values).

For quantitative analysis of time-resolved microscope images, the emission signal intensity was calculated according to the equation: $S = (\mu_{signal}\text{-}\mu_{bckg})$, where, μ_{signal} is equal to the mean pixel gray value in a region of interest (ROI) corresponding to the area of a cell, and μ_{bckg} is equal to the mean pixel gray value in a nearby ROI of equivalent area, (Fig. S3). The donor-normalized LRET signal (LRETN) was defined as S_{520}/S_{540}, where S_{520} was the net LRET signal measured through a narrow-pass filter that collected only a portion of the GFP emission ($\lambda_{em} = 520 \pm 10$ nm) and S_{540} represented a signal that comprised sensitized GFP emission and directly excited terbium emission ($\lambda_{em} = 540 \pm 10$ nm). Cells were selected for analysis that exhibited both GFP expression and loading of TMP-Lumi4 as determined by examining corresponding continuous wave fluorescence images ($\lambda_{ex} = 480 \pm 20$ nm, $\lambda_{em} = 535 \pm 25$ nm) and time-resolved images of terbium emission ($\lambda_{ex} = 365$ nm, $\lambda_{em} = 540 \pm 10$ nm). Intramolecular LRETN was calculated for cells expressing GFP-eDHFR. Intermolecular LRETN was calculated for cells expressing interacting proteins (ZO-1/PDZ1-eDHFR and GFP-cldn1/tail) and for cells expressing putatively noninteracting proteins (ZO-1/PDZ1-eDHFR and GFP-cldn1/tail$^{\Delta YV}$). The mean, standard deviation and range of LRETN was determined for each sample. *P*-value was determined from a two-tailed, two-sample, unequal variance t-test of the interacting and putatively noninteracting, intermolecular LRETN samples (Table S3).

Luminescent lifetime estimation and calculation of in vitro LRET energy transfer efficiency. Stock solutions of TMP-Lumi4 and Lumi4®-Tb were chelated with terbium, diluted to ~20 nM in assay buffer (50 mM K_2HPO_4, KH_2PO_4, 18 mM β-mercaptoethanol, 10 μM NADPH, pH 7.2). Fluorescence intensity was measured using a time-resolved fluorescence plate reader (Perkin Elmer, Victor 3V) with 340 nm excitation (60 nm bandpass) and 545 nm emission (10 nm bandpass). Intensity values (500 μs integration) were measured at different time delays from 100 μs to 2500 μs (100 μs increments). Plots of intensity vs. delay time were fit to a single exponential with KaleidaGraph v4.0 (Fig. S1), and lifetime was estimated from the equation: $I(t) = I_0 \exp(-t/\tau)$ (4). The measurements were repeated 3× to yield mean estimated lifetimes: Lumi4®-Tb, 2.35 ± 0.05 ms (mean ± s.e.m.); TMP-Lumi4, 2.28 ± 0.07 ms (mean ± s.e.m.).

To measure the lifetime of terbium-sensitized GFP emission, TMP-Lumi4 and GFP-eDHFR were diluted to 20 nM and 100 nM, respectively in assay buffer (50 mM K_2HPO_4, KH_2PO_4, 18 mM β-mercaptoethanol, 10 μM NADPH, pH 7.2). Lifetime was determined by single exponential fit to plots of intensity (340 nm exciation, 520 nm emission) vs. delay time (Fig. S1). Three repetitions yielded the mean estimated lifetime of terbium-sensitized GFP emission: 0.78 ± 0.04 ms (mean± s.e.m.).

The efficiency of energy transfer from terbium-to-GFP in the TMP-Lumi4/GFP-eDHFR complex was calculated from the equation, $E = 1 - \tau_A/\tau_D$, where τ_A is the lifetime of sensitized GFP emission and τ_D is the lifetime of TMP-Lumi4 (5). From lifetime data, a value of 0.67 was calculated.

1. Rajapakse HE, Reddy DR, Mohandessi S, Butlin NG, Miller LW (2009) Luminescent terbium protein labels for time-resolved microscopy and screening. *Angew Chem Int Ed Engl* 48(27):4990–4992.

2. Miller LW, Cai Y, Sheetz MP, Cornish VW (2005) In vivo protein labeling with trimethoprim conjugates: A flexible chemical tag. *Nat Methods* 2(4):255–257.

3. Grunwald D, Shenoy SM, Burke S, Singer RH (2008) Calibrating excitation light fluxes for quantitative light microscopy in cell biology. *Nat Protoc* 3(11):1809–1814.
4. Lakowicz JR (2006) Principles of fluorescence spectroscopy, 3rd ed. (Springer, New York), p. 99.
5. Selvin PR, Hearst JE (1994) Luminescence energy transfer using a terbium chelate: Improvements on fluorescence energy transfer. *Proc Natl Acad Sci USA* 91(21): 10024–10028.

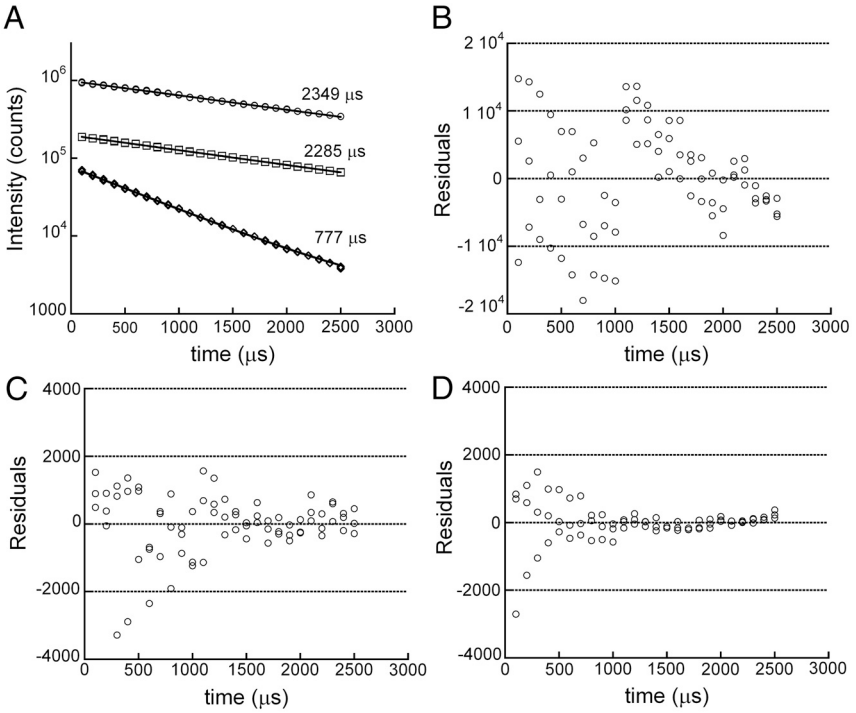

Fig. S1. Results of emission lifetime analyses. (*A*) Representative intensity vs. time plots of Lumi4-Tb (circles), TMP-Lumi4 (squares) and terbium-sensitized GFP emission from a TMP-Lumi4/GFP-eDHFR complex (diamonds), measured as described in *SI Materials and Methods*. For Lumi4-Tb and TMP-Lumi4, the solid line is a single exponential (2 parameter) fit to the data, $I(t) = I_0 \exp(-t/\tau)$. For sensitized GFP emission, the data were fit to a single exponential decay with an offset (3 parameter), $I(t) = A + I_0 \exp(-t/\tau)$. The calculated lifetime is shown adjacent to the plotted curves, and three repetitions of the experiment yielded values that agreed within <4 percent. The 3 parameter fit for the sensitized emission curve yielded an offset value <2% of the amplitude in all cases. The r^2 residuals were greater than 0.99 in call cases, and residual plots showed no structure. (*B*)–(*D*) Residual plots for Lumi4-Tb, TMP-Lumi4, and sensitized GFP emission, respectively.

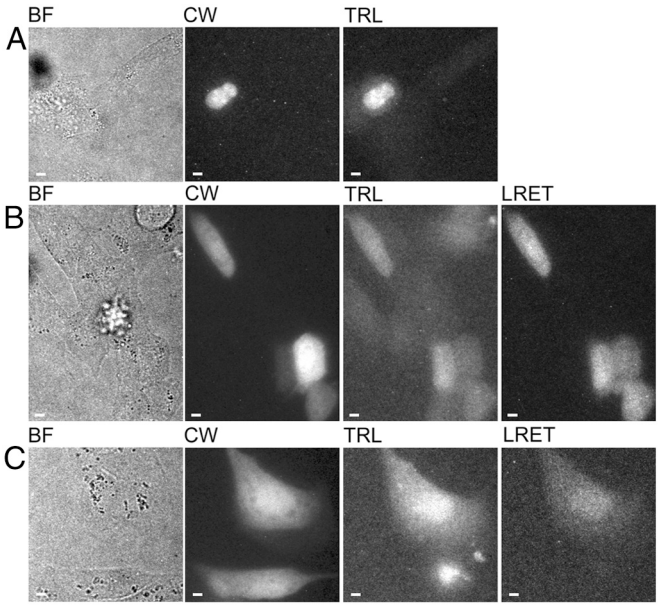

Fig. S2. Additional images showing that both SLO-mediated membrane permeabilization and osmotic lysis of pinocytic vesicles can be used to deliver TMP-Lumi4 to the cytoplasm of at least two cell types: NIH3T3 fibroblasts and MDCKII epithelial cells. Upon delivery into cells, TMP-Lumi4 binds specifically to eDHFR fusion proteins, and the specific binding can be visualized by time-resolved luminescence microscopy. Micrographs: BF, bright field; CW, continuous-wave fluorescence ($\lambda_{ex} = 480 \pm 20$ nm, $\lambda_{em} = 535 \pm 25$ nm); TRL, time-resolved fluorescence ($\lambda_{ex} = 365$ nm, $\lambda_{em} > 400$ nm, gate delay $= 10$ μs); LRET, time-resolved LRET ($\lambda_{ex} = 365$ nm, $\lambda_{em} = 520 \pm 10$ nm, gate delay $= 10$ μs). Scale bars, 10 μm. (*A*) NIH3T3 fibroblast cells transiently cotransfected with DNA encoding nucleus-localized CFP and nucleus-localized eDHFR were incubated with TMP-Lumi4 (15 μM) and streptolysin O (SLO, 50 ng/mL) for 10 min. Time-resolved detection of broadband (>400 nm) terbium emission reveals localization of TMP-Lumi4 in nucleus of transfected cell (corresponding to continuous wave fluorescence image of CFP emission). (*B*) NIH3T3 fibroblast cells transiently transfected with DNA encoding GFP-eDHFR. Cells were incubated in hypertonic medium containing TMP-Lumi4 (50 μM) for 10 min. to allow pinocytosis and subsequently exposed to hypotonic medium to effect lysis of pinocytic vesicles and release of probe into the cytoplasm. Time-resolved detection of broadband emission (>400 nm) reveals terbium luminescence in TMP-Lumi4-loaded cells. Luminescence resonance energy transfer (LRET) is seen only in transfected cells (indicated in continuous wave fluorescence image) coincidentally loaded with TMP-Lumi4 when visualized in time-resolved mode through a narrow-pass filter (520 ± 10 nm), indicating specific labeling of the GFP-eDHFR fusion protein. (*C*) MDCKII cells coexpressing ZO-1/PDZ1-eDHFR and GFP-cldn1/tail were incubated with TMP-Lumi4 (15 μM) and streptolysin O (SLO, 50 ng/mL) for 10 min. Terbium-to-GFP LRET is seen only in transfected cells loaded with TMP-Lumi4.

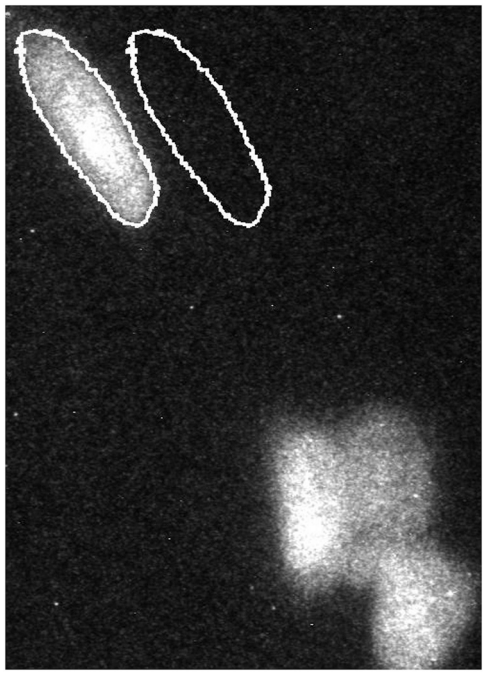

Fig. S3. Representative regions of interest (ROIs) used to calculate LRET signal levels as described in *SI Materials and Methods*.

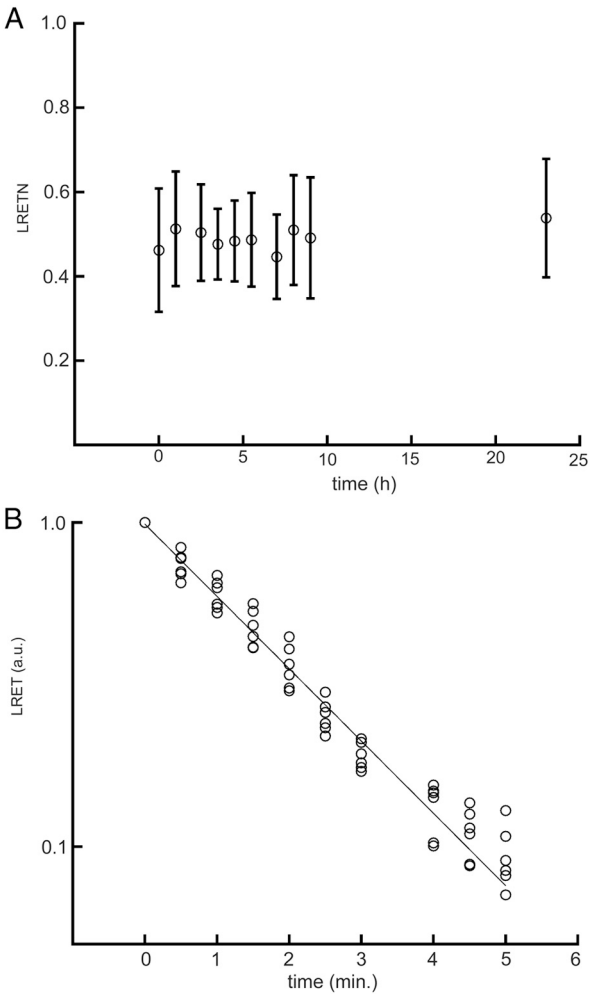

Fig. S4. TMP-Lumi4 is stably luminescent in cells and resistant to photobleaching. (*A*) Plot of mean ± s.d., donor-normalized LRET signal (LRETN) vs. time obtained from time-resolved images of MDCKII cells expressing GFP-eDHFR and pinocytically loaded with TMP-Lumi4. LRETN equals the 520 nm/540 nm emission signal ratio, where emission signal was measured as the background-subtracted mean gray value for a single cell in an image. More than 10 cells were used to calculate mean LRETN at each time point. (*B*) Semilog plot of LRET signal intensity (normalized to initial value at $t = 0$) vs. accumulated irradiation time for MDCKII cells expressing GFP-eDHFR and pinocytically loaded with TMP-Lumi4. A field of view was exposed to continuous wave LED excitation at the standard illumination intensity (~0.6 W/cm^2), imaged at successive timepoints ($\lambda_{ex} = 365$ nm, $\lambda_{em} = 520 \pm 10$ nm, gate delay = 10 μs), and the background-subtracted mean gray value determined for each cell exhibiting LRET in the field. The solid line is a single exponential (2 parameter) fit to the data, $y = a^* \exp(-t/\tau)$. For the data shown, $\tau = 1.95 \pm 0.05$ min and $r^2 = 0.98$. The experiment was performed 3 times, and τ ranged from 1.9–2.1 min. with $r^2 > 0.97$ in all cases ($n > 5$ cells for each experiment). Specific imaging parameters are provided in Table S2.

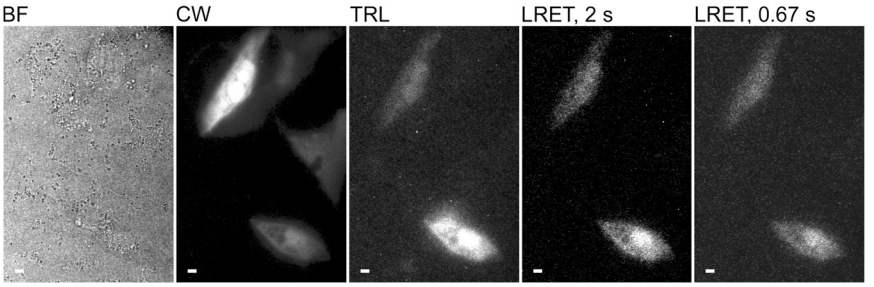

Fig. S5. Rapid detection of intermolecular LRET between TMP-Lumi4-labeled ZO-1/PDZ1-eDHFR and GFP-cldn1/tail. MDCK cells coexpressing ZO-1/PDZ1-eDHFR and GFP-cldn1/tail. Cells were loaded by pinocytosis (10 min) of culture medium containing TMP-Lumi4 (60 μM) followed by osmotic lysis of pinosomes. Micrographs: BF, bright field; CW, continuous wave fluorescence ($\lambda_{ex} = 480 \pm 20$ nm, $\lambda_{em} = 535 \pm 25$ nm); TRL, time-resolved fluorescence ($\lambda_{ex} = 365$ nm, $\lambda_{em} > 400$ nm, gate delay = 10 μs); LRET, time-resolved images ($\lambda_{ex} = 365$ nm, $\lambda_{em} = 520 \pm 10$ nm, gate delay = 10 μs) acquired in a single frame of indicated length. Both LRET images were adjusted to identical contrast levels (50/300 min/max). Scale bars, 10 μm.

Table S1. Summary of Live-Dead Assay™ (Invitrogen, L3224) assessment of the effects of SLO and osmotic lysis of pinosomes on MDCKII and NIH3T3 cells, 2 h posttreatment

	MDCK		NIH3T3	
	SLO	Pinocytosis	SLO	Pinocytosis
Total	691	1521	927	1056
Live (%)	657 (95.08)	1423 (93.56)	878 (94.71)	992 (93.94)
Dead (%)	34 (4.92)	98 (6.44)	49 (5.29)	64 (6.06)

Table S2. Summary of detection and image processing parameters for all time-resolved images and data presented in the paper

Image or data	λ_{em} (nm)	Excitation events	Frame length (ms)	Frames	Acquisition time (ms)	Intensifier gain (V)	Pixel dimensions	Pixel depth	Contrast (min / max)*
Fig. 3*A*, TRL	>400	220	666	1	666	778	500 × 500	1024	150/1000
Fig. 3*A*, TRL + TMP	>400	220	666	1	666	778	500 × 500	1024	150/1000
Fig. 3*B*, TRL	>400	110	333	4	1333	833	500 × 700	4096	316/4092
Fig. 3*B*, LRET	510–530	330	1000	4	4000	833	500 × 700	4096	150/1000
Fig. 4*A*, TRL	>400	110	333	4	1066	778	750 × 750	4096	510/2952
Fig. 4*A*, LRET	510–530	660	2000	4	8000	778	750 × 750	4096	150/1000
Fig. 4*A*, LRET + TMP (2 min)	510–530	660	2000	4	8000	778	750 × 750	4096	150/1000
Fig. 4*A*, LRET + TMP (20 min)	510–530	660	2000	4	8000	778	750 × 750	4096	150/1000
Fig. 4*B*, TRL	>400	220	666	4	2667	778	750 × 750	4096	722/4078
Fig. 4*B*, LRET	510–530	660	2000	4	8000	778	750 × 750	4096	150/1000
Table S3	†	660	2000	4	8000	889	N/A	4096	N/A
Fig. S2*A*, TRL	>400	220	666	1	666	778	500 × 500	1024	93/1020
Fig. S2*B*, TRL	>400	110	333	4	1333	778	500 × 700	4096	396/4092
Fig. S2*B*, LRET	510–530	660	2000	4	8000	778	500 × 700	4096	130/2223
Fig. S2*C*, TRL	>400	110	333	8	1333	889	500 × 500	8192	907/4154
Fig. S2*C*, LRET	510–530	660	2000	4	8000	922	500 × 500	4096	150/1500
Fig. S4*A*	†	330	1000	4	4000	833	N/A	4096	N/A
Fig. S4*B*	510–530	660	2000	4	8000	889	N/A	4096	N/A
Fig. S5, TRL	>400	44	133	1	133	778	600 × 900	1024	61/1019
Fig. S5, LRET, (2 s)	510–530	330	1000	2	2000	778	600 × 900	2048	50/300
Fig. S5, LRET, (0.67 s)	510–530	110	333	2	666	778	600 × 900	2048	50/300

*Contrast indicates minimum and maximum gray level values used to represent respective images.
†For quantitative analysis of donor-normalized LRET signals (presented in Table S3 and Fig. S4*A*), 2 images were acquired using the indicated source/camera parameters: acceptor emission (510–530 nm) and donor emission + acceptor emission (530–550 nm).

Table S3. Summary of donor-normalized LRET (LRETN) data* for cells expressing interacting (ZO-1/PDZ1-eDHFR and GFP-cldn1/tail) and noninteracting (ZO-1/PDZ1-eDHFR and GFP-cldn1/tail$^{\Delta YV}$) proteins

	ZO-1/PDZ1-eDHFR GFP-cldn1/tail	ZO-1/PDZ1-eDHFR GFP-cldn1/tail$^{\Delta YV}$
No. cells	11	9
Mean	0.38	0.06
S.d.	0.10	0.04
Range	0.17–0.50	0.02–0.11
t-test *p* value = 3.4×10^{-7}†		

*Calculated as described in the main article and in *SI Materials and Methods* from time-resolved images acquired using parameters listed in Table S2.
†Calculated from a two-tailed, two-sample, unequal variance *t*-test of the interacting and putatively noninteracting LRETN samples.